Macromolecular Bioscience
www.mbs-journal.de

Chelating Polymers for Hereditary Hemochromatosis Treatment

Ondřej Groborz, Lenka Poláková, Kristýna Kolouchová, Pavel Švec, Lenka Loukotová, Vijay Madhav Miriyala, Pavla Francová, Jan Kučka, Jan Krijt, Petr Páral, Martin Báječný, Tomáš Heizer, Radek Pohl, David Dunlop, Jiří Czernek, Luděk Šefc,* Jiří Beneš, Petr Štěpánek, Pavel Hobza, and Martin Hrubý**

Hemochromatosis (iron overload) encompasses a group of diseases that are characterized by a toxic hyperaccumulation of iron in parenchymal organs. Currently, only few treatments for this disease have been approved; however, all these treatments possess severe side effects. In this study, a paradigm for hemochromatosis maintenance/preventive therapy is investigated: polymers with negligible systemic biological availability form stable complexes with iron ions in the gastrointestinal tract, which reduces the biological availability of iron. Macroporous polymer beads are synthesized with three different iron-chelating moieties (benzene-1,2-diol, benzene-1,2,3-triol, and 1,10-phenanthroline). The polymers rapidly chelate iron ions from aqueous solutions in vitro in the course of minutes, and are noncytotoxic and nonprooxidant. Moreover, the in vivo biodistribution and pharmacokinetics show a negligible uptake from the gastrointestinal tract (using ^{125}I-labeled polymer and single photon emission computed tomography/computed tomography), which generally prevents them from having systemic side effects. The therapeutic efficacy of the prepared polymers is successfully tested in vivo, and exhibits a significant inhibition of iron uptake from the gastrointestinal tract without any noticeable signs of toxicity. Furthermore, an in silico method is developed for the prediction of chelator selectivity. Therefore, this paradigm can be applied to the next-generation maintenance/preventive treatment for hemochromatosis and/or other diseases of similar pathophysiology.

1. Introduction

Hemochromatosis (also known as iron overload) occurs when iron uptake exceeds its excretion from the body and in the long term leads to its toxic accumulation in the organism. Progressive iron accumulation predominantly occurs in liver, pancreas, joints, skin, heart, and the gonadotrophin-secreting cells of the pituitary.[1] Without any treatment, iron overload can cause an increase in pigmentation, hepatic fibrosis, diabetes mellitus, arthropathy, cardiomyopathy, or hypogonadotropic hypogonadism.[1,2] Moreover, patients with untreated hemochromatosis have a significantly increased risk of liver cirrhosis and hepatocellular carcinoma.[3]

The acquired (secondary) hemochromatosis can be associated with thalassemia[4] (if treated with frequent blood transfusions), chronic alcoholism, or other conditions. The hereditary (primary) hemochromatosis is the most common form of iron overload.[5,6] As there is no known physiological pathway to excrete excessive iron

O. Groborz, Dr. L. Poláková, K. Kolouchová, P. Švec, Dr. L. Loukotová, Dr. J. Kučka, Dr. J. Czernek, Dr. P. Štěpánek, Dr. M. Hrubý
Institute of Macromolecular Chemistry
Czech Academy of Sciences
Heyrovského náměstí 2, 162 06 Prague 6, Czech Republic
E-mail: ondrej.groborz@seznam.cz; mhruby@centrum.cz

O. Groborz
Department of Organic Chemistry
Faculty of Science
Charles University
Hlavova 8, 128 43 Prague 2, Czech Republic

O. Groborz, Prof. J. Beneš
Institute of Biophysics and Informatics
First Faculty of Medicine
Charles University
Salmovská 1, 120 00 Prague 2, Czech Republic

The ORCID identification number(s) for the author(s) of this article can be found under https://doi.org/10.1002/mabi.202000254.

DOI: 10.1002/mabi.202000254

K. Kolouchová, P. Švec
Department of Physical Chemistry
Faculty of Science
Charles University
Hlavova 8, 128 43 Prague 2, Czech Republic

Dr. V. M. Miriyala, Dr. R. Pohl, Dr. D. Dunlop, Prof. P. Hobza
Institute of Organic Chemistry and Biochemistry
Czech Academy of Sciences
Flemingovo náměstí 542/2, 162 06 Prague 6, Czech Republic

Dr. P. Francová, Dr. P. Páral, Dr. M. Báječný, Dr. T. Heizer, Dr. L. Šefc
Center for Advanced Preclinical Imaging (CAPI)
First Faculty of Medicine
Charles University
Salmovská 3, 120 00 Prague 2, Czech Republic
E-mail: sefc@cesnet.cz

Dr. J. Krijt
Institute of Pathophysiology
First Faculty of Medicine
Charles University
U Nemocnice 5, 128 53 Prague 2, Czech Republic

out of the body,[7] the only way to control the iron concentration in the body is by its uptake regulations.[2,8] An impaired iron uptake regulation is most commonly related to an insufficient hepcidin-mediated downregulation of ferroportin.[9,10] The worldwide prevalence of the C282Y mutation of HFE gene[11] (associated with the most common hereditary hemochromatosis, type 1)[12,13] is 1:200–400,[2,11,14] and locally can be as high as 1:13 people.[15,16,17] The clinical presentation of the symptoms usually occurs in middle-aged patients, when the patients have already accumulated a large amount of iron in their organs.[2,14]

Currently, the main approach to hereditary hemochromatosis treatment is phlebotomy.[18] This method involves the removal of 450–500 mL twice a month to twice a week until the serum iron levels are reduced to the required values.[19] However, the established methodology of determining the endpoint and the frequency of therapeutic phlebotomy is limited.[7] For the time being, as a maintenance therapy for the hereditary hemochromatosis (or preventive treatment if a person is known to be a C282Y-homozygote),[20] phlebotomy can be performed several times a year, but cannot be indicated in some patients (most common reason being trypanophobia, nonsideropenic anemia, and hemophilia).[20] Low-iron diet is also recommended for iron level maintenance; nevertheless, the efficacy is limited due to the iron ubiquity.[7] Nowadays, a more common approach in maintenance therapy is an iron chelators therapy.[7,21] The obsolete chelator deferoxamine (Desferal) has unvafourable unfavorable pharmacokinetics (fast clearance and must be parenterally administered due to its poor per os biological availability) and causes severe side effects, such as ophthalmic and auditory toxicity, increased risk of bacterial and fungal infections, hematological changes, and allergic and dermatological reactions.[22] The state-of-the-art, per os-administrable FDA- and EMA-approved iron chelators deferiprone (Ferriprox) and deferasirox (Desirox, Exjade) are rather efficient; however, their pharmacokinetics are far from ideal and they cause severe side effects as well, such as thrombocytopenia, agranulocytosis, neutropenia, hepatic fibrosis, renal damage, and gastrointestinal bleeding, and they have a considerably high drug-induced mortality drug-induced mortality rate in patients.[23,24,25,26]

There are essentially three common forms of iron in the common Western diet: first, the vast majority of the iron in food occurs in the oxidation state Fe^{3+}; second, a minor amount of iron appears in the Fe^{2+} state; and third, the porphyrine-chelated form (heme) is relatively commonly present (mainly in meat).[27] A natural equilibrium exists between Fe^{3+} and Fe^{2+} oxidation states, as these ions can be oxidized by atmospheric oxygen or reduced in food.[28] Only Fe^{2+} and heme (hemin) forms of iron are biologically available; the uptake of the most common iron form Fe^{3+} is very poor, and therefore, it must be reduced before its absorption.[28] An increased uptake of ascorbic acid, lactate, or other reducing agents leads to an increased Fe^{2+} concentration in the gastrointestinal tract, which increases the biological uptake of iron.[29] Likewise, an increased uptake of molecules that form stable complexes with iron ions (e.g., phytates or tannic acid) causes a decrease in iron uptake.[30]

A relatively new paradigm for the maintenance (or preventive) therapy of hereditary hemochromatosis has been proposed: polymers/particles with negligible systemic biological availability form stable complexes with iron ions in the gastrointestinal tract, which decreases the biological availability of iron. The nonabsorbability and nondegradability of these polymers prevents systemic side effects or toxicity. Although a few pilot experiments on model systems have been described in the literature as a proof-of-concept,[31,32,33] there are still unanswered questions and unresolved problems that we try to answer in this full story study.

Most importantly, all previous studies investigate the biological effect of chelators with a high affinity toward Fe^{3+}, but very low affinity toward Fe^{2+}. As was described above, the vast majority of inorganic iron ions are, indeed, present in form of Fe^{3+}, however, only Fe^{2+} is biologically available. We have compared the biological efficiency polymers bearing Fe^{3+} and both Fe^{2+}/Fe^{3+} binding moieties; our results indicate that if Fe^{2+} ions are chelated as well, the biological effect is considerably improved.

Secondly, both nanoparticles and gel-like dendrimers were suggested as chelator carriers in previous studies. Both nanoparticles and non-crosslinked polymers can accumulate in the body (either in intestines or even enter the blood circulation) over the long period of uptake required for lifelong maintenance therapy. This could cause severe adverse effects or induce pathologies in patients. Therefore, we suggest the usage of highly porous iron-chelating microparticles, the biodistribution of which we have shown in subchronic study in mice. Our data suggests that this material is nonabsorbable from the GIT and still reasonably biologically active. Furthermore, our carrier polymer forms a depot in the stomach which releases the polymer slowly over a course of several days (signal in stomach was detectable even 3 days after the administration). This might also be beneficial for the intended application because it prolongs the contact of polymer with the food.

Thus, we improve the already existing paradigm in terms of long-term safety and efficiency. We investigate the in silico and in vitro chelating selectivity, kinetics, oxidant behavior, in vivo/ex vivo distribution in mice, and most importantly its efficiency and safety. This study could be considered as a guide for further rational development of better chelating polymers for maintenance therapy of hemochromatosis and/or diseases with similar pathology.

2. Experimental Section

2.1. Materials

The 1,10-phenanthroline-5-amine was purchased from Puralab s.r.o, (Běchovice, Czech Republic). All solvents, anhydrous sodium sulfate, ammonium iron(II) sulfate hexahydrate, hydrogen peroxide, and formaldehyde solution were purchased from Lach:Ner s.r.o., (Neratovice, Czech Republic). The radioactive sodium iodide $Na^{125}I$ was purchased from M.G.P. s.r.o. (Zlín, Czech Republic). Fluorescein was purchased from Fluka (Buchs, Switzerland). All other chemicals were purchased from Sigma-Aldrich Ltd. (Prague, Czech Republic). All chemicals were used without any additional purification procedures unless stated otherwise.

2.2. Instruments and Methods

The ^{13}C solid-state NMR (ssNMR) spectra were measured using the JEOL 600 MHZ EZC600R spectrometer (^{13}C resonance frequency of 150.9 MHz) in a 3.2 mm rotor. Spectra were acquired using the cross-polarization magic angle spinning technique: acquisition time 0.0433 s, FID size: 2048, 23.5–24.0 °C temperature range, and the spinning rate of 18 kHz. The number of scans were varied from 4100 to 93 100. The NMR spectra were processed in MestReNova 6.0.2 (Mestrelab Research, S.L., Santiago de Compostela, Spain), and FID was apodized with 20 Hz exponential function. Fourier transform infrared (FT-IR) spectra were measured using the attenuated total reflectance (ATR) technique on a spectrometer Spectrum 100T FT-IR (Perkin-Elmer, USA) with a DTSG detector fitted with a Universal ATR accessory with a diamond/ZnSe crystal. All FT-IR spectra were acquired in the range 650–4000 cm^{-1} at 16 scans. Elemental analysis was performed on a Perkin-Elmer Series II CHNS/O Analyzer 2400 (PE Systems Ltd., Czech Republic) instrument. The bead size distribution (weighted by volume fraction) was determined by Mie scattering (Mastersizer 3000 instrument, Malvern Instruments Ltd., United Kingdom). The structure and morphology of the prepared polymers were analyzed using scanning electron microscopy (SEM) Quanta 200 FEG (FEI Company, Hillsboro, USA). The samples were dried and coated with a thin layer of metallic gold by sputter coater Desk II (Denton Vacuum, Moorestown, USA) prior to the SEM measurement. Inductively coupled plasma mass spectrometry with tandem configuration (ICP-MS-MS) was conducted on Agilent 7700 in helium mode (inert gas flow was 4.1 mL min^{-1}) (Agilent, Santa Clara, USA). Internal calibration was employed (calibrated on control samples without the addition of the polymer). Atomic absorption spectrophotometry was measured on Perkin Elmer, model 3110 (Perkin-Elmer Inc., Waltham, USA). External calibration was utilized.

2.3. Polymer Synthesis

2.3.1. Poly(glycidyl methacrylate-co-ethylene glycol dimethacrylate) (G-Gel)

Poly(*N*-vinyl pyrrolidone) (8.00 g, 22.2 µmol, M_w = 360 000 g mol^{-1}) and sodium nitrite (0.40 g, 5.80 mmol) were dissolved in distilled water (400 mL) in a 1 L round bottom flask. Afterward, lauryl alcohol (98.0 g, 526 mmol), cyclohexanol (10.0 g, 100 mmol), ethylene glycol dimethacrylate (5.40 g, 5.1 mL, 27 mmol), glycidyl methacrylate (102.9 g, 95.7 mL, 725 mmol), and 2,2′-azobis(2-methylpropionitrile) (AIBN, 0.50 g, 3.04 mmol) were added to the flask. The flask was subsequently flushed with nitrogen, and the mixture was vigorously stirred at 70 °C for 2 h, followed by heating at 80 °C for the next 6 h. After the reaction, the polymer was filtered, washed thoroughly with water, ethanol, methanol, and diethyl ether, and then dried in air at 55 °C. The product was isolated as a fine, white powder.

FT-IR: 3499 (w), 3059 (w), 2993 (m), 2940 (m), 2887 (sh), 1723 (s), 1482 (m), 1447 (m), 1386 (m), 1339 (w), 1255 (m), 1237 (sh), 1169 (sh), 1148 (s), 1129 (m), 1071 (m), 994 (m), 965 (sh), 905 (m), 842 (m), and 757 (m) cm^{-1} (Figure S6, Supporting Information). ^{13}C-ssNMR (151 MHz), δ (ppm): 175.7, 65.6, 54.1, 47.4, 43.3, and 14.5 (Figure S7, Supporting Information). Elemental analysis: C 58.30 ± 0.03%, H 6.91 ± 0.00%, N below LOQ, and Cl below LOQ.

2.3.2. Poly[2-hydroxy-3-(N-methylamino)propyl methacrylate-co-ethylene glycol dimethacrylate] (Methylamino-G-Gel)

G-gel (1.00 g, 6.70 mmol of epoxide groups) and 40% aqueous methylamine solution (3.50 mL, 45 mmol) were put into a 10 mL flask. The reaction mixture was stirred for 3 days at room temperature. Afterward, the polymer was filtered off and thoroughly washed with phosphate-buffered saline (PBS), 5% hydrochloric acid, water, ethanol, methanol, and diethyl ether, and then dried in air at 55 °C. The product was isolated as a fine, white powder.

FT-IR: 3249 (vw), 2955 (m), 2271 (vw), 1719 (s), 1460 (s), 1391 (m), 1261 (m), 1147 (s), 1109 (sh), 1060 (sh), 992 (w), 960 (w), and 880 (w) cm^{-1} (Figure S8, Supporting Information). ^{13}C-ssNMR (151 MHz), δ (ppm): 175.9, 64.3, 52.6, 43.5, 33.2, and 15.8 (Figure S9, Supporting Information). Elemental analysis: C 46.95 ± 0.10%, H 7.23 ± 0.33%, N 4.11 ± 0.08%, and Cl 12.06%.

2.3.3. Poly[2-hydroxy-3-(N,N-dimethylamino)propyl methacrylate-co-ethylene glycol dimethacrylate] (Dimethylamino-G-Gel)

G-gel (120 mg, 0.80 mmol of epoxide groups) and 2.0 M dimethyl methylamine solution in THF (5.00 mL, 10.0 mmol) were added into a 10 mL flask. The reaction mixture was stirred for 3 days at room temperature. Afterward, the polymer was filtered off and washed thoroughly with PBS, 5% hydrochloric acid, water, ethanol, methanol, and diethyl ether, and then dried on air at 55 °C. The product was isolated as a fine, white powder.

FT-IR: 3234 (vw), 2955 (m), 2688 (w), 2469 (m), 1721 (s), 1641 (m), 1469 (s), 1389 (m), 1389 (m), 1389 (m), 1264 (m), 1246 (m), 1148 (s), 1115 (m), 1060 (m), 986 (m), 961 (m), 935 (sh), 883 (w), and 748 (m) cm^{-1} (Figure S10, Supporting Information). ^{13}C-ssNMR (151 MHz), δ (ppm): 176.4, 63.0, 55.1, 43.5, 41.0, and 16.1 (Figure S11, Supporting Information). Elemental analysis: C 45.62 ± 0.21%, H 8.10 ± 0.11%, N 4.73 ± 0.09%, and Cl 13.21%.

2.3.4. Poly[2-hydroxy-3-(N-(2,3-dihydroxybenzyl)(N-methyl)amino) methacrylate-co-ethylene glycol dimethacrylate] (CAT)

Methylamino-G-gel polymer (102 mg, 299 µmol of amine groups), anhydrous sodium sulfate (680 mg, 4.80 mmol), catechol (70 mg, 636 µmol), and methanol (1.50 mL) were added to a 25 mL flask. Subsequently, 40% aqueous solution of formaldehyde (0.375 mL, 5.44 mmol) were added in one portion, and the flask was sealed and stirred with a magnetic stir bar at room temperature for 7 days. Afterward, the polymer was filtered and thoroughly washed with PBS, 5% hydrochloric acid, water, ethanol, methanol, and diethyl ether, and then dried in air at 55 °C. The product was isolated as a fine, off-white to beige powder, pink to orange when wet.

FT-IR: 3282 (vw), 2994 (w), 2944 (m), 1720 (s), 1656 (vw), 1459 (m), 1388 (m), 1253 (m), 1146 (s), 1065 (sh), 991 (w), 960 (m), 877 (m), and 748 (m) cm^{-1} (Figure S12, Supporting Information). ^{13}C-ssNMR (151 MHz), δ (ppm): 175.4, 144.5, 119.4, 63.0, 53.7, 43.8, 33.1, and 17.8 (Figure S13, Supporting Information). Elemental analysis: C 50.87 ± 0.03%, H 7.26 ± 0.04%, N 2.64 ± 0.02%, and Cl 7.76%.

2.3.5. Poly[2-hydroxy-3-(N-(2,3,4-trihydroxybenzyl)(N-methyl) amino) methacrylate-co-ethylene glycol dimethacrylate] (GAL)

GAL polymer was prepared by analogous procedure as CAT polymer. Here, pyrogallol (82 mg, 651 µmol) was added instead of catechol. The product was isolated as a fine, slightly purple powder, dark purple to brown when wet.

FT-IR: 3282 (vw), 2985 (w), 2955 (w), 1720 (s), 1625 (m), 1456 (m), 1387 (m), 1365 (sh), 1252 (s), 1448 (s), 1112 (sh), 1059 (sh), 992 (w), 960 (sh), 874 (w), and 749 (m) cm^{-1} (Figure S14, Supporting Information). ^{13}C-ssNMR (151 MHz), δ (ppm): 175.5, 141.9, 131.1, 116.7, 63.0, 53.8, 43.7, 32.6, and 17.9 (Figure S15, Supporting Information). Elemental analysis: C 52.65 ± 0.09%, H 6.77 ± 0.08%, N 2.28 ± 0.08%, and Cl 5.61%.

2.3.6. Poly[2-hydroxy-3-(N-(1,10-phenanthroline-5-yl)amino)propyl methacrylate-co-ethylene glycol dimethacrylate] (FEN)

G-gel (210 mg, 1.41 mmol of epoxide groups), 1,10-phenanthroline-5-amine (900 mg, 4.61 mmol), and ethylene glycol (20 mL) were added to a 25 mL flask. The suspension was flushed with nitrogen, sealed, and heated at 75 °C for 3 days. Afterward, the mixture was filtered and the polymer washed thoroughly with PBS, 5% hydrochloric acid, water, ethanol, methanol, and diethyl ether, and then dried in air at 55 °C. The product was isolated as a fine, red to cocoa-like powder.

FT-IR: 3409 (vw), 2982 (w), 2935 (m), 2893 (m), 2834 (w), 1721 (s), 1652 (m), 1619 (w), 1598 (m), 1550 (w), 1472 (sh), 1450 (s), 1386 (m), 1369 (m), 1327 (w), 1250 (s), 1152 (sh), 1130 (sh), 1108 (s), 992 (m), 963 (m), 921 (sh), 849 (m), 749 (m), and 720 (m) cm^{-1} (Figure S16, Supporting Information). ^{13}C-ssNMR (151 MHz), δ (ppm): 175.7, 144.3, 132.8, 121.9, 72.6, 66.4, 57.4, 54.1, 43.5, and 14.6 (Figure S17, Supporting Information). Elemental analysis: C 55.37 ± 0.06%, H 7.22 ± 0.11%, N 1.76 ± 0.06%, and Cl 2.28%.

2.3.7. ^{125}I-Labeled CAT Polymer

G-gel (550 mg, 3.69 mmol of epoxide groups), tyramine (20.0 mg, 146 µmol), and methanol (1.00 mL) were added to a 25 mL flask. The reaction mixture was stirred at room temperature for 24 h. The mixture was filtered and washed with water and methanol. The insoluble residue was mixed with 40% aqueous solution of methylamine (5.0 mL, 64 mmol), and stirred for 3 days. The polymer was filtered off, washed with water, ethanol, and methanol, and then dried. In a 2 mL vial, this polymer (51.5 mg) and chloramine-T (10.0 mg, 44 µmol) were mixed with PBS (400 µL). $Na^{125}I$ (373 MBq, 100 µL aqueous solution) was added. The mixture was stirred for 2 h. Afterward, fresh ascorbic acid solution (5.2 mg, 30 µmol in 200 µL of water) was added, the mixture was centrifuged for 10 min, and the supernatant was decanted and replaced with the same portion of fresh ascorbic acid solution and PBS solution (1.00 mL). The mixture was stirred for 5 min, and the polymer was washed two more times following the previous procedure. The final washing was performed overnight with methanol and then twice with ultrapure water to obtain pure labeled polymer (323 MBq, 91% radiochemical yield).

This polymer was reacted with formaldehyde and catechol according to a previously described CAT synthesis to obtain ^{125}I-labeled CAT polymer (276 MBq, 94% radiochemical yield). The ^{125}I-label stability was tested by suspending a polymer sample (≈1 MBq) in PBS solution at room temperature; after 72 h, the polymer was filtered off. No significant activity was detected in the supernatant.

2.4. In Silico Calculations

Quantum chemical calculations were performed to quantify the enthalpic stability of chelator complexes with Fe^{2+}, Fe^{3+}, Cu^{2+}, and Zn^{2+} ions. All ions were represented as hexaaqua-ions, except for Cu^{2+}, which was represented as tetraaqua-ion. The *N*-methyl-capped monomeric chelator moieties representations ([CAT], [GAL], and [FEN]) and complexes with different degrees of protonation were represented as shown in Figures S1 and S2 in the Supporting Information.

All molecules were optimized in their ground state at high level density functional theory (DFT) using the dispersion corrected DFT-D3/B97D/TZVPP[34] in aqueous medium (ε_r = 78.5)[35] and the implicit solvent model COSMO. All calculations were performed using TURBOMOLE 6.6 interface[36] and automatized in the CUBY4 framework.[37]

The chelation energy was calculated according to Equations (1b), (2b), (3b), or (4b). The results are shown in Table S1 in the Supporting Information

$$[\mathrm{CHELATOR}]^{+} + \mathrm{M(H_2O)}_n^{+X} \rightarrow [\mathrm{CHELATOR}]\mathrm{MH_2(H_2O)}_{n-2}^{+X+1} + 2\mathrm{H_2O} \quad (1a)$$

$$\Delta H = H_{[\mathrm{CHELATOR}]\mathrm{MH_2(H_2O)}_{n-2}^{+X+1}} + 2H_{\mathrm{H_2O}} - H_{[\mathrm{CHELATOR}]^{+}} - H_{\mathrm{M(H_2O)}_n^{+X}} \quad (1b)$$

$$[\mathrm{CHELATOR}]^{+} + \mathrm{M(H_2O)}_n^{+X} \rightarrow [\mathrm{CHELATOR}]\mathrm{MH(H_2O)}_4^{+X} + \mathrm{H_3O^{+}} + \mathrm{H_2O} \quad (2a)$$

$$\Delta H = H_{[\mathrm{CHELATOR}]\mathrm{MH(H_2O)}_{n-2}^{+X}} + H_{\mathrm{H_3O^{+}}} + H_{\mathrm{H_2O}} - H_{[\mathrm{CHELATOR}]^{+}} - H_{\mathrm{M(H_2O)}_n^{+X}} \quad (2b)$$

$$[\mathrm{CHELATOR}]^{+} + \mathrm{M(H_2O)}_n^{+X} \rightarrow [\mathrm{CHELATOR}]\mathrm{M(H_2O)}_{n-2}^{+X-1} + 2\mathrm{H_3O^{+}} \quad (3a)$$

$$\Delta H = H_{[\mathrm{CHELATOR}]\mathrm{M(H_2O)}_{n-2}^{+X}} + 2H_{\mathrm{H_3O^+}} - H_{[\mathrm{CHELATOR}]^+} - H_{\mathrm{M(H_2O)}_n^{+X}} \quad (3b)$$

$$[\mathrm{CHELATOR}] + \mathrm{M(H_2O)}_n^{+X} \rightarrow [\mathrm{CHELATOR}]\mathrm{M(H_2O)}_{n-2}^{+X} + 2\mathrm{H_2O} \quad (4a)$$

$$\Delta H = H_{[\mathrm{CHELATOR}]\mathrm{M(H_2O)}_{n-2}^{+X}} + 2H_{\mathrm{H_2O}} - H_{[\mathrm{CHELATOR}]} - H_{\mathrm{M(H_2O)}_n^{+X}} \quad (4b)$$

where $[\mathrm{CHELATOR}]^+$ represents $[\mathrm{CAT}]^+$, $[\mathrm{GAL}]^+$, or [FEN] (refer to Figures S1 and S2 in the Supporting Information), M represents metal ion with charge $+X$, and n represents the number of water molecules coordinated to the complex.

The enthalpy gain of each chelator with different ions was then used to estimate the chelation selectivity.

2.5. In Vitro Characterization

2.5.1. In Vitro Iron Chelation Capacity Study

Ammonium iron(II) sulfate hexahydrate (245.5 mg, 626.1 µmol) was dissolved in ultrapure water (100 mL). The pH was adjusted with hydrochloric acid to 2.00 or 4.00. 1.000 mL of this solution was added to the chelating polymer (10.00 mg) and vigorously stirred. After 2, 5, 10, or 25 min, the polymer was filtered, and the supernatant was collected. To each supernatant, 10% aqueous nitric acid was added (1.00 mL), and the iron concentration was determined using atomic absorption spectroscopy (AAS).

Analogously, a solution of iron(III) nitrate hexahydrate was prepared (248.9 mg, 616.0 µmol in 100 mL of ultrapure water) and the pH was adjusted to 2.00. Subsequently, the chelation kinetics was measured according to the previously mentioned procedure.

All obtained data were fitted using Origin 2019 (version 9.6.0.172, OriginLab Corporation, Northampton, USA) to the functional form given by Equation (5)

$$m_{\mathrm{Fe},t} = m_{\max} \cdot \left(1 - \mathrm{e}^{-k \cdot t}\right) \quad (5)$$

where $m_{\mathrm{Fe},t}$ is the chelated iron mass per gram of the polymer, $m_{\max}$ is the total iron chelation capacity per gram of the polymer, k is the rate constant, and t is the chelation time.

2.5.2. In Vitro Ion Chelation Selectivity Study

The polymer chelation selectivity was measured. Calcium nitrate tetrahydrate (5.89 g, 25.0 mmol), copper acetate (2.12 mg, 11.7 µmol), iron(III) nitrate nonahydrate (57.9 mg, 14.3 µmol), magnesium chloride (1.57 g, 7.71 mmol), manganese sulfate tetrahydrate (9.34 mg, 41.9 µmol), and zinc chloride (22.9 mg, 168 µmol) were dissolved in ultrapure water (500 mL). The pH was adjusted to 2.00 by the addition of hydrochloric acid. The chelating polymer (CAT, GAL, or FEN; 13.6 mg) was added to the prepared solution (50 mL) and the mixture was stirred for 72 h. A control group was prepared analogously but no polymer was added.

Ammonium iron(II) sulfate hexahydrate (61 mg, 156 µmol), zinc(II) sulfate heptahydrate (35 mg, 121 µmol), and copper(II) sulfate pentahydrate (6.3 mg, 25.2 µmol) were dissolved in 250 mL of degassed water and pH was adjusted to 2.00 with the addition of hydrochloric acid. Then, 2.5 mL of this solution was mixed with GAL (14.6 mg, 47 µmol chelator moieties), CAT (14.6 mg, 43 µmol of chelator moieties), methylamino-G-gel (14.6 mg, 43 µmol of amine moieties), or FEN (39.1 mg, 16 µmol of chelator moieties). The mixture was flushed with argon, sealed, and stirred for 45 min at room temperature. Afterward, the mixture was filtered and the aliquot (750 µL) was mixed with 15% nitric acid (250 µL).

Metal ion concentrations were determined in the supernatant using ICP-MS-MS. The polymer selectivity for Fe ion was calculated using Equation (6)

$$S_{\mathrm{x}} = \frac{c_{\mathrm{Fe_{control}}} - c_{\mathrm{Fe_{final}}}}{c_{\mathrm{x_{control}}} - c_{\mathrm{x_{final}}}} \cdot \frac{c_{\mathrm{x_{final}}}}{c_{\mathrm{Fe_{final}}}} \quad (6)$$

where $c_{\mathrm{Fe_{control}}}$ is the iron ion concentration in the control experiment; $c_{\mathrm{x_{control}}}$ is the investigated ion concentration in the control experiment; $c_{\mathrm{Fe_{final}}}$ is the iron ion concentration after absorption and $c_{\mathrm{x_{final}}}$ is the concentration of the investigated ion in the solution after absorption.

2.5.3. Antioxidant Properties

Antioxidant behavior of the prepared polymers in the presence of hydrogen peroxide and in vitro generated peroxyl radicals was determined. Fluorescein solution (2.4×10^{-5} M in PBS, pH = 6.8) was prepared and stored in a refrigerator. This solution exhibited stable values of fluorescence intensity during several weeks.

In the experiments employing hydrogen peroxide, PBS (900 µL) and the previously prepared fluorescein solution (27 µL) were added to Eppendorf tubes with the corresponding amounts of polymer samples. The tubes were placed in a heating block block, and the polymers were incubated at 37 °C for 60 min. Then, hydrogen peroxide aqueous solution (30% w/w, 900 µL) was added, and the tubes were shaken and heated to 37 °C throughout the reaction. At certain time intervals, the tubes were opened, the polymer was filtered (0.45 µm filter), and fluorescence intensity of the supernatant was measured (λ_{ex} = 485 nm, λ_{em} = 518 nm).The experiments were performed in triplicates.

Scavenging activities of the polymers against in vitro generated peroxyl radicals were determined by the following procedure: six 2 mL Eppendorf tubes with the corresponding amount of the polymer were placed into a heating block heated to 37 °C. The fluorescein solution (300 µL) and PBS (1.4 mL) were added, and the polymer was incubated in this mixture for 60 min. The reaction was then started by the addition of freshly prepared 2,2′-azobis-(2-amidinopropane) hydrochloride (AAPH) solution in PBS (100 µL, 460×10^{-3} M). Throughout the reaction, the tubes were shaken and heated to 37 °C. At predetermined time intervals, the tubes were opened, the polymer was filtered (0.45 µm filter), and fluorescence intensities of the clear filtrates were determined. All measurements were performed in triplicate and the results were averaged. The extent of the scavenging activity (A_t) was calculated using Equation (7)

$$A_t = \frac{I_t - I_{0,t}}{1 - I_{0,t}} \cdot 100 \quad (7)$$

where A_t is the scavenging activity at certain reaction time t, and $I_{0,t}$ and I_t are the relative intensities of fluorescence of the blank sample and of the tested sample, respectively, at time t.

2.5.4. Cytotoxicity

Normal human dermal fibroblast (NHDF) cells were cultured in Dulbecco's Modified Eagle Medium (DMEM) with the addition of 10% fetal bovine serum and 1% penicillin streptomycin in humidified atmosphere that contained 5% CO_2 and subcultivated when 80% confluency was attained.

CAT, FEN, GAL, or methylamino-G-gel (100 mg) was suspended in ultrapure water (700 µL). The suspensions were stirred at room temperature for 72 h. Afterward, the polymer beads were separated via centrifugation, and the supernatant was subsequently filtered via a 0.22 µm syringe filter.

NHDF cells were precultivated for 24 h in 96-well plates (density 1.0×10^{-4} cells cm^{-2}). The cells were incubated with polymer beads aqueous extracts for 48 h, and the cell viability was determined via a 3-(4,5-dimethylthiazol-2-yl)-2,5-diphenyltetrazolium bromide (MTT) assay. The tetrazolium bromide is reduced to formazan in mitochondria of living cells, and thus, the cell viability can be spectrophotometrically determined at 570 nm after cell lysis (sodium dodecyl sulfate lysis buffer). The cells were observed and documented before lysis using phase-contrast light microscopy (Olympus IX71 with camera DP74, Tokyo, Japan). The MTT assay results were compared with the control samples (the addition of water instead of polymer beads aqueous extracts), and these samples were determined to have a cell viability of 100%. The results were presented as the mean values of three independent experiments.

2.6. In Vivo Experiments

The experiments described here were performed in accordance with Act No. 359/2012 Sb. on the protection of animals against cruelty and decree 419/2012 Sb. Ministry of Agriculture on the protection of experimental animals (including relevant EU regulations).

All in vivo experiments were performed using C57BL/6N strain female mice (8 weeks old, purchased from Velaz s.r.o, Prague, Czech Republic). They were housed in accordance to the approved guidelines (in individually ventilated cages with the sterilized bedding, 12:12 h light–dark cycle at 22 ± 1 °C and 60 ± 5% humidity), and feed and water were provided ad libitum. Mice feed was provided by Altromin Spezialfutter GmbH (Lage, Germany).

2.6.1. Biodistribution of the per os Administered Polymer per os

The ^{125}I-labeled CAT polymer was administered via a probe into the stomachs of four mice (a suspension in 200 µL water/≈65 MBq per mouse). The polymer biodistribution was analyzed in an ALBIRA positron emission tomography/single photon emission computed tomography/computed tomography (PET/SPECT/CT) system (Bruker Biospin, Ettlingen, Germany) equipped with a multipinhole collimator at different time intervals. Animals, anesthetized with isoflurane (3.0% initial concentration, 1.5–2.0% maintenance concentration, purchased from Baxter S.A., Lessines, Belgium), were placed in the prone position for image acquisition. Afterward, the exact biodistribution profile was determined ex vivo by measuring the organ activity (stomach, small intestine, colon, kidneys, liver, heart, spleen, and lungs) and blood sample using the VDC-404 detector (Veenstra Instruments, Joure, The Netherlands).

2.6.2. Preparation of Mice Feed

The concentration of iron, copper, and zinc in both mice feeds (Altromin 1324 Velaz and Altromin C 1038) were determined by State Veterinary Administration of the Czech Republic (Státní veterinární ústav, Prague, Czech Republic). The used methods were consistent with the norm ČSN EN ISO/IEC 17025:2005.[38] The Altromin 1324 Velaz feed contained 367.50 ± 40.42 mg of iron per kilogram, 11.60 ± 1.74 mg of copper per kilogram, and 80.90 ± 12.14 mg of zinc per kilogram. Iron-deficient mice feed, Altromin C 1038, contained 9.70 ± 1.06 mg of iron per kilogram, 6.02 ± 0.90 mg of copper per kilogram, and 27.60 ± 4.14 mg of zinc per kilogram.

These two types of mice feed, Altromin 1324 Velaz (maintenance diet) and Altromin C 1038 (low iron diet), were ground into a fine powder and mixed to resemble iron composition in human diet. The CAT polymer (5.85 g kg^{-1} feed, 17.1 mmol of chelating moieties) and the FEN polymer (15.63 g kg^{-1} feed, 6.6 mmol of chelating moieties) were added to this mixture. These feed mixtures were moisturized, thoroughly mixed into a paste, formed into small pellets, and dried at 55 °C overnight.

2.6.3. Iron Uptake Suppression with the Prepared Polymers (Efficacy Test)

Mice were randomly divided into 3 groups (n = 6), and they were fed with the prepared diets that had the polymer addition: CAT group, FEN group, and control group (fed with the prepared feed mixture without any polymer addition). Their weight, hematocrit, and hemoglobin levels were monitored every 4 to 7 days. During the first four blood samplings, 500 µL of blood was collected to lower the iron content in the body. Every following blood sample had a volume of 50 µL. On day 41, the animals were sacrificed and their kidneys, heart, stomach, small intestine, colon, and spleen were examined for any histological abnormalities and pathology in at least 3 independent animals per group. The organs were fixed in 10% buffered formaldehyde solution and embedded in paraffin. Serial sections (5.0 µm) were subsequently prepared and stained with standard hematoxylin-eosin staining protocol.

Dean-Dixon's Q-test was applied to reject the outlier values, and statistical significance was examined using the analysis of variance test performed with Origin 9.6.0.172 (OriginLab Corporation, Northampton, USA).

3. Result and Discussion

3.1. Polymer Synthesis and Characterization

Macroporous insoluble crosslinked poly(glycidyl methacrylate-*co*-ethylene glycol methacrylate) (G-gel) beads were prepared by a modified procedure according to Švec et al.[39] via a suspension radical polymerization of glycidyl methacrylate with ethylene glycol dimethacrylate as a crosslinking agent. The product was a fine, free flowing powder, no particles were visible with an unaided eye. These polymer crosslinkages ensured its nonsolubility, and therefore, the polymer's biological availability is restricted. The G-gel was characterized by FT-IR, which showed strong bands at 900 and 1720 cm^{-1}, which corresponds to the presence of epoxide moieties and ester moieties, respectively (Figure S6, Supporting Information). The presence of ester groups was also confirmed by solid-state NMR (^{13}C-ssNMR, signal at 175 ppm; Figure S7, Supporting Information).

Since very small particles could potentially be absorbed from the gastrointestinal tract (GIT), spherical particles with the diameter greater than 5 μm are required for the application. In the aqueous environment, G-gel forms particles larger than 15 μm, while a majority of them was in the range from 25 to 90 μm (**Figure 1**A). Moreover, the particle shape was investigated using SEM (Figure 1B,C). The majority of particles were round spheres, and only a few irregularities were detected. No particles with sharp edges were observed, which is important because sharp fragments may irritate the epithelial cells of the GIT, whereas spherical structures were not expected to cause any mechanical damage.

The reactive epoxide groups present in the G-gel were further chemically modified in such a way that the final products contain iron-chelating moieties (**Figure 2**A). First, G-gel was reacted with methylamine or dimethylamine to form secondary amine and tertiary amine, respectively. The structures of methylamino-G-gel and dimethylamino-G-gel were confirmed using FT-IR (Figures S8 and S10, Supporting Information) and ^{13}C ssNMR (Figures S9 and S11, Supporting Information). Second, the FEN polymer was prepared by reaction with 1,10-phenanthroline-5-amine and characterized (Figures S16 and S17, Supporting Information). Then, the amine group in the methylamino-G-gel was modified using the Betti reaction to covalently bind the chelating agent (catechol or pyrogallol), which produced the CAT and GAL polymers. These polymers were also characterized using FT-IR and ^{13}C ssNMR (Figures S12–S15, Supporting Information). The molar amount of particular functional groups was calculated from the elemental composition

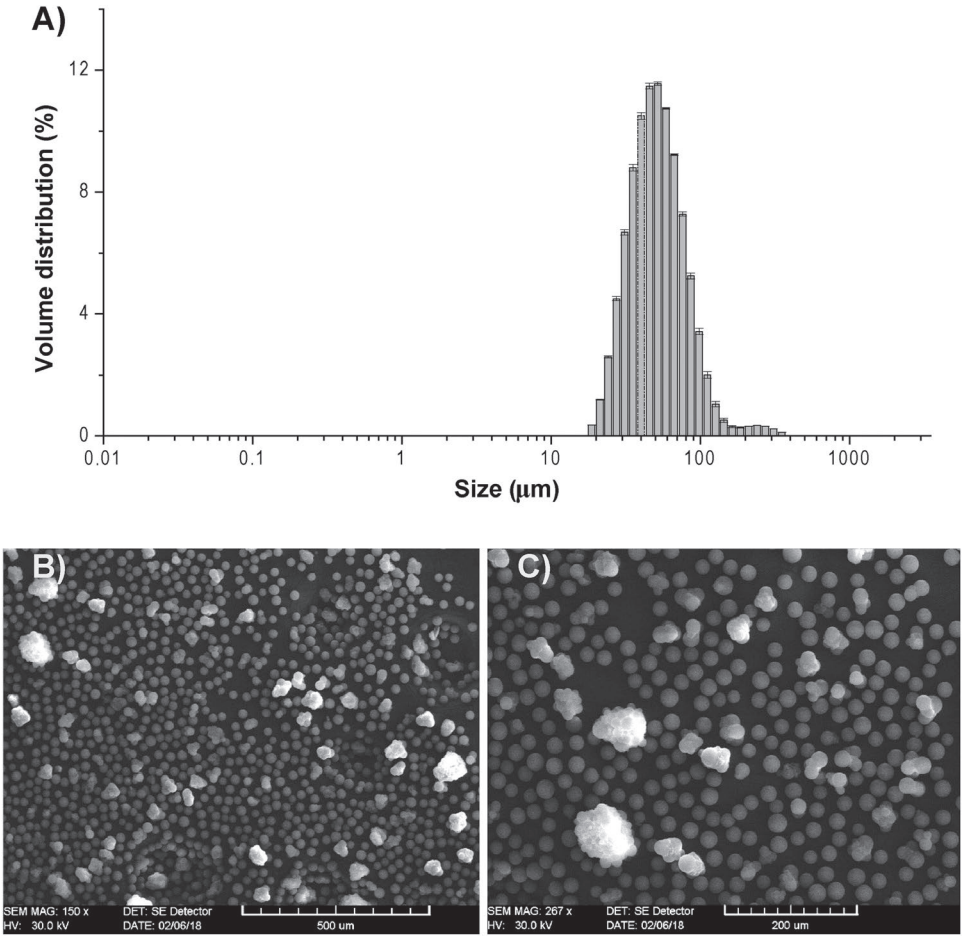

Figure 1. A) The particles size histogram of G-gel (Mie scattering) in water ($c \approx 1$ mg mL^{-1}), B,C) SEM images of typical G-gel particles with two different magnifications: 150-fold and 267-fold.

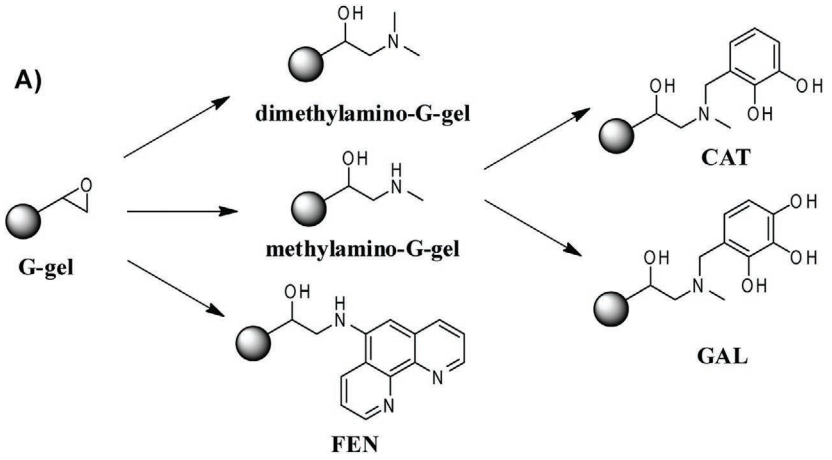

B)

Polymer	moiety	mmol / g
G-gel	epoxide	670
methylamino-G-gel	amine	2.93 ± 0.11
dimethylamino-G-gel	amine	3.37 ± 0.12
FEN	catechol	0.42 ± 0.03
GAL	pyrogallol	3.21 ± 0.43
CAT	phenanthroline	2.92 ± 0.27

Figure 2. A) Scheme of the polymer synthesis; the bead represents crosslinked polymer backbone of poly(glycidyl methacrylate-*co*-ethylene glycol methacrylate). All prepared polymers were isolated and stored in the form of hydrochloride salts. B) Calculated molar amount of the particular functional groups per gram of each polymer.

of each polymer (Equations (S1)–(S4), Supporting Information; Figure 2B). For CAT and GAL, the values are comparable (≈3 mmol g^{-1}). The FEN contents lower molar amounts of the chelator group, which may be due to the steric hindrance of relatively larger substituents (1,10-phenanthroline moiety compared to methyl) and the lower nucleophilicity of the aromatic amine moiety.

To monitor the polymer in vivo biodistribution, the radioactive ^{125}I-labeled CAT polymer was prepared using a different synthetic strategy, as CAT could not be labeled with radioactive iodine directly using a simple electrophilic iodination ($Na^{125}I$ and chloramine-T). The in situ generated intermediates can oxidize catechol groups, and thus, the polymer labelling would have only minor yields due to this side reaction. First, G-gel was reacted with a small portion of tyrosine (4% of the total epoxide groups). This amount was sufficient for further radio-isotope labelling, but was not sufficient for significantly changing the physicochemical properties of the polymer. Subsequently, the tyrosine-labeled G-gel was reacted with an excess of methylamine and subsequently labeled with the radioactive iodine ^{125}I (91% radiochemical yield). Last, this polymer was reacted with formaldehyde and catechol to form ^{125}I-labeled CAT.

3.2. In Silico Calculations

The chelation energies of Fe^{2+}, Fe^{3+}, Cu^{2+}, and Zn^{2+} ions were calculated. For each complex, ground states were determined (for Fe^{2+} quintet; for Fe^{3+} sextet, for Cu^{2+} doublet, and for Zn^{2+} singlet). All cations were represented as metal ions surrounded by a corresponding number of explicitly defined water molecules. The dielectric constant of a diluted hydrochloric acid, which is the main component of gastric acid, is similar to the dielectric constant of water.[35] All ions, chelators representations ([CAT], [GAL], and [FEN]; see Figures S1 and S2 in the Supporting Information) and chelator-ion complexes were optimized, and subsequently their energy was determined. The complexation energies were calculated according to Equations (1) to (4); the results are listed in Table S1 in the Supporting Information. Note that the complexation energy was calculated in implicit solvent and the values for the explicit solvent can be slightly lower (especially for H_3O^+). This may explain why monoprotonated complexes seem to have higher chelation energies than double-protonated or triple-protonated complexes. Therefore, the specific values presented in Table S1 in the Supporting Information should be interpreted with caution. However, these values can be employed to compare the affinities of each chelator species to each cation, as the discussed effect is cancelled when the values are compared.

The results suggest that complex protonation decreases the complex stability (compare di- and triprotonated complexes); in other words, the chelating ability of our chelators might decrease with decreasing pH values.

The calculated values were used to rank the affinity of each ligand toward each ion (**Table 1**). The in silico data suggests that both [GAL] and [CAT] should selectively chelate Fe^{3+} ions out of the investigated ions, and Cu^{2+}, Zn^{2+}, and Fe^{2+} should be chelated to a considerably smaller degree. Under some conditions, Cu^{2+} can also form a stable complex with [CAT] ligand. However, this complexation has been observed to occur only in basic conditions[40] as [CAT] becomes deprotonated at higher pH. These conditions are not relevant for our intentions; therefore, [CAT] can be considered as a selective chelator under the conditions in GIT. [FEN] exhibits a very high affinity to all ions, especially toward Cu^{2+} ion but also toward Fe^{3+} and Fe^{2+} and Zn^{2+}. Although [FEN] is not very selective, unlike [CAT] and [GAL], it can be expected to significantly lower the concentration of Fe^{2+} ions, which has substantially higher biological availability.

Table 1. Calculated rank of ion affinities to each chelator representation [FEN] for FEN polymer, [GAL] for GAL polymer, and [CAT] for CAT polymer.

Chelator	Affinity rank
[FEN]	$Cu^{2+} \gg Fe^{3+} > Fe^{2+} > Zn^{2+}$
[GAL]	$Fe^{3+} \gg Fe^{2+} > Zn^{2+} > Cu^{2+}$
[CAT]	$Fe^{3+} \gg Fe^{2+} > Zn^{2+} > Cu^{2+}$

Table 2. Fe^{2+} ion and Fe^{3+} ion chelation capacities of each polymer at the given pH.

	m_{max} (mg of iron per g of polymer)			
Ion	Fe^{2+}		Fe^{3+}	
pH	2.00	4.00	2.00	4.00
FEN	0.09 ± 0.01	4.4 ± 0.2	2.3 ± 0.1	ND[a)]
GAL	2.3 ± 0.2	16.1 ± 1.3	10.9 ± 0.6	ND
CAT	1.7 ± 0.1	16.4 ± 1.4	15.6 ± 0.9	ND

[a)]ND: not determined.

3.3. In Vitro Characterization

3.3.1. Iron Chelation Capacity and Selectivity

The iron-chelation capacity and selectivity of the prepared polymers were investigated because these properties are essential for the intended applications. First, the polymer chelation capacity for Fe^{2+} ions and Fe^{3+} ions was studied at pH = 2.00 and 4.00 (these pH values were chosen to represent the environment of the human gastrointestinal tract for the different conditions; however, higher pH values would interfere with measurement due to salts precipitation, see below). The exception is for Fe^{3+} ions in the solution at pH = 4.00 because this solution was not stable in the long-term: a precipitation of iron(III) hydroxide appeared upon preparation and interfered with the chelation measurements. The chelation kinetics (Figure S3, Supporting Information) showed that the chelation of both Fe^{2+} ions and Fe^{3+} ions is very fast, in the course of minutes. Moreover, the total chelation capacity of Fe^{2+} ions was noticeably higher at higher pH for all polymers (**Table 2**), which may be caused by the competition between iron chelation and a protonation of the polymer-bound ligand at lower pH. The lower total chelation capacity of FEN is due to its lower molar amount of chelator groups per gram (Figure 2B). The observed chelation kinetics and iron-chelation capacity of the prepared polymers are suitable for the proposed application.

Experiments to determine the chelation capacities and chelation selectivities at higher pH (including pH 6.0 and 8.0) were performed, but the results were not reproducible. Both Fe^{2+} and Fe^{3+} were at those pH values very prone to precipitate out due to the hydrolysis regardless of the chelating polymer's presence and thus, no relevant data could be obtained.

This result indicates that $[Fe(H_2O)_6]^{2+}$ and $[Fe(H_2O)_6]^{3+}$ ions, which we are able to chelate, can occur only in acidic solutions in stomach. In basic solutions, they precipitate to form insoluble hydrolysis products with negligible biological availability. Therefore, the key question when investigating the chelator efficacy in the GIT is whether or not it works in slightly acidic to acidic solutions.

The high iron-chelation selectivity is essential due to the presence of other metal ions in feed which are necessary for the human body. Therefore, the chelation selectivity of Fe^{2+} and Fe^{3+} over other ions (Cu^{2+}, Zn^{2+}, Mn^{2+}, Ca^{2+}, and Mg^{2+}) in concentrations relevant to the human food composition at pH = 2.00 was studied. The ions were incubated with the polymers, and their concentrations were subsequently assessed by ICP-MS-MS. If the decrease in the iron ions concentration after the incubation with the chelating polymer was significant, the polymer was considered to be able to chelate this ion. If the competitor ion concentration was statistically lower after the incubation, the chelation selectivity was calculated using Equation (6). The results are compiled in **Table 3**. All polymers were shown to reduce the concentrations of Fe^{3+} ions, however, only FEN significantly reduced the concentration of Fe^{2+} ions. CAT and GAL polymers were very selective for the chelation of Fe^{3+} ions to which they exhibited a very high affinity. A very slight chelation was observed for Cu^{2+} in CAT and GAL when no Fe^{3+} was present and only Fe^{2+} was in the solution, however, this effect was nearly negligible. FEN exhibited a high affinity toward Cu^{2+} and lower affinity toward Zn^{2+} ion. As expected, methylamino-G-gel, which was utilized as a control polymer, exhibited no significant affinity to any of the tested ions.

Importantly, the results of quantum chemical calculations are in a full qualitative agreement with the in vitro data. This shows that in silico predictions can be usefully employed in rational design of chelating polymers.

3.3.2. Antioxidant Properties

The prepared polymers were designed to exhibit adhesiveness to the wall of the GIT (especially the stomach) to prolong their presence in GIT and increase the iron chelation efficacy. With respect to the desired prolonged contact of the polymers with the gastric mucous layer, the polymers should not contribute to oxidative damage of the GIT tissue. Therefore, the polymers should not increase the rate of reactive oxidative species (ROS) generation (pro-oxidative properties), and, if possible, should

Table 3. The polymer selectivity of Fe^{2+} and Fe^{3+} ions chelation over Mg^{2+}, Ca^{2+}, Mn^{2+}, Cu^{2+}, or Zn^{2+} ions at pH 2.00. Selectivity was calculated with Equation (6). * indicates that no statistically significant decrease in ion concentration was observed in the solution due to the chelation.

Polymer	Ion	Chelation?	Ca^{2+}	Mg^{2+}	Cu^{2+}	Zn^{2+}	Mn^{2+}
FEN	Fe^{2+}	Yes	*	*	<0.01	0.3 ± 0.0	*
	Fe^{3+}	Yes	*	*	<0.01	*	*
GAL	Fe^{2+}	No	*	*	(0.6 ± 0.4)	*	*
	Fe^{3+}	Yes	*	*	*	*	*
CAT	Fe^{2+}	No	*	*	(0.2 ± 0.5)	*	*
	Fe^{3+}	Yes	*	*	*	*	*

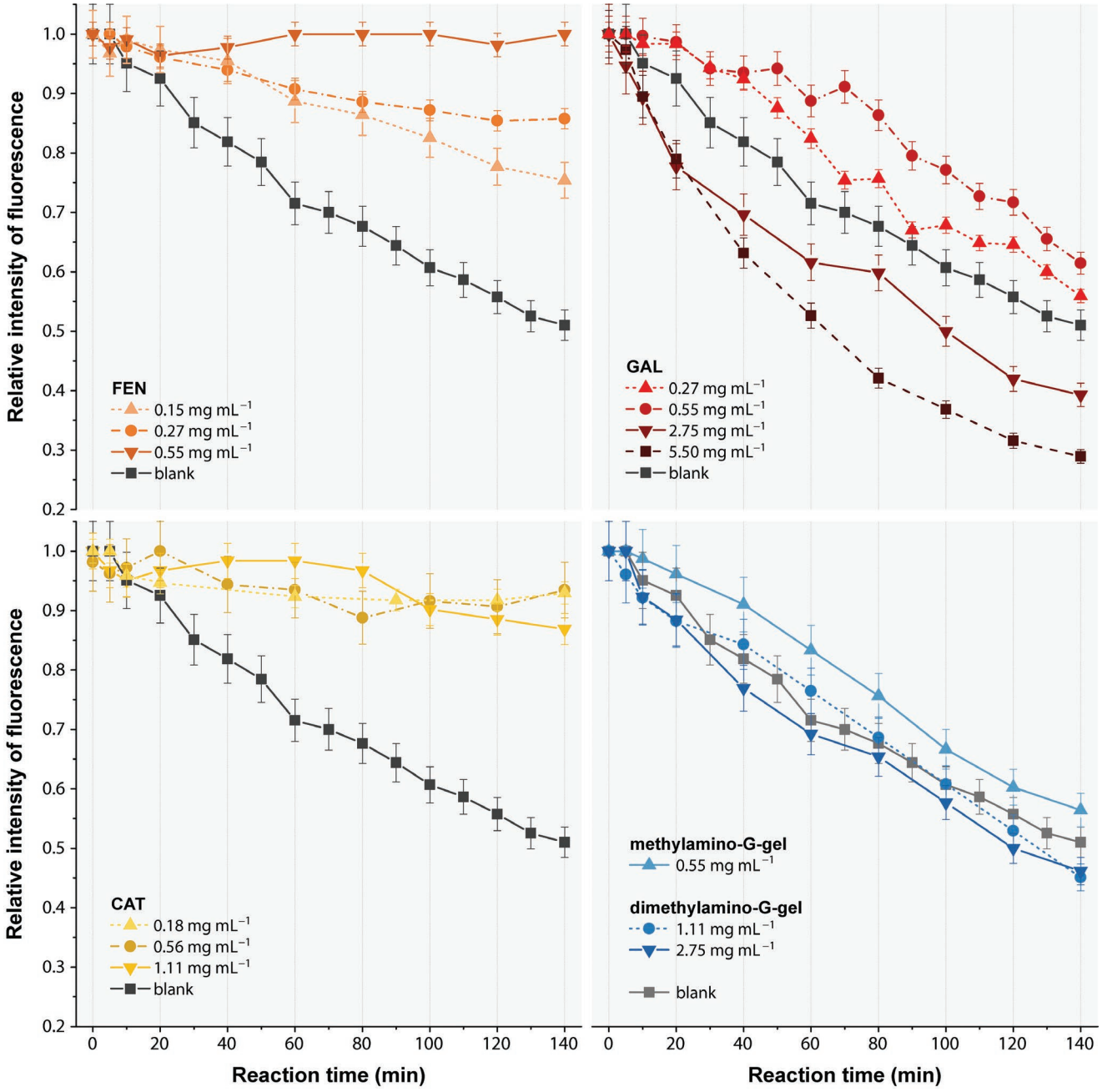

Figure 3. Time-dependence of relative fluorescein fluorescence intensity in the presence of hydrogen peroxide and polymers at various concentrations: FEN, GAL, CAT, and neat matrices. Average values from three independent experiments are presented.

have antioxidant properties to prevent oxidative damage of the gastrointestinal tract by the potentially generated ROS.

Hydrogen peroxide occurs in normal metabolism in mammalian cells and is a key metabolite of oxygen in aerobic metabolism of cells and tissues. Hydrogen peroxide is a weak oxidizing agent that may directly damage lipids, proteins, DNA, or enzymes which contain reactive thiol groups.[41–43] Although hydrogen peroxide negligibly penetrates cell membranes, it can be transported via common aquaporin transporters in the cell membranes.[44] Therefore, hydrogen peroxide formed in one location may diffuse a considerable distance before it decomposes to a highly reactive hydroxyl radical and damage the surrounding tissues.

To determine the polymer behavior in the presence of hydrogen peroxide and the products of its decomposition, in vitro hydrogen peroxide scavenging assay was carried out. Here, the formed radicals oxidize fluorescein to nonfluorescent products, decreasing the fluorescence intensity. It was found that whereas FEN showed a concentration-dependent behavior over the measured concentration range, giving the complete fluorescein protection at 0.55 mg mL^{-1} during the whole measurement period (**Figure 3**A), neat methylamino-G-gel

matrix without bound chelator exhibited at the same concentration no ability to protect fluorescein against the oxidative effect of hydrogen peroxide (Figure 3D). This observation indicates that 1,10-phenanthroline bound to this type of polymeric network behaved as an antioxidant in the presence of hydrogen peroxide; to the best of our knowledge, this phenomenon has not been reported.

Moreover, the comparison of polymers with phenolic chelators revealed that the number of chelator phenolic moieties had a substantial role in this assay. Neat polymer matrix (dimethylamino-G-gel; Figure 3D) showed no changes in the fluorescence intensity, whereas a significant decrease was observed for the GAL polymer at concentrations higher than 0.55 mg mL^{-1} (compared with the blank sample; Figure 3B), which suggests that GAL acted as a pro-oxidant under the given conditions. In contrast, excellent scavenging ability was noted for CAT polymer (Figure 3C), where the catechol moiety is capable of eliminating nucleophile hydroperoxyl anions and hydroxyl radicals (predominantly formed in experimental conditions of the assay), which causes a termination of these reactive species. As a result, the fluorescence intensity remained almost unchanged during the whole reaction time even at very low polymer concentration (0.18 mg mL^{-1}).

Among the oxygen-containing radicals, peroxyl radicals are the most concerning, as they are rather reactive toward cell membranes, which subsequently causes its destruction, cytoplasm leakage, and cell death.[45] In vivo life-time of peroxyl radicals is on the order of seconds, which enables them to migrate relatively far from their site of formation. These radicals cause severe damage and inflammation of the surrounding tissue.[45]

Peroxyl radicals were generated by a standard in vitro procedure that utilizes thermal decomposition of AAPH at 37 °C. Likewise, the antioxidant properties can be quantified with fluorimetry (Figure S4, Supporting Information).[46] In general, the scavenging activities of polymers containing chelators increased with the increasing concentration. This finding was the most pronounced for FEN, having 47% at 0.6 mg mL^{-1} and 97% at 2.8 mg mL^{-1} after the first 20 min. Considering that neat polymer matrix that contains secondary amine groups (methylamino-G-gel) exhibited almost no activity to scavenge peroxyl radicals, the scavenging activities of FEN can be attributed to the presence of covalently bound 1,10-phenanthroline. This finding is quite surprising; since it has not yet been reported in literature that 1,10-phenanthroline in both low molecular weight and polymeric forms possesses antioxidant activity against peroxyl radicals. Moreover, scavenging activity of the 1,10-phenanthroline polymer was substantially higher than those for the polymers with polyphenols (46% and 58% at 2.8 mg mL^{-1} of CAT and GAL polymer, respectively, after the first 20 min). Especially at higher polymer concentrations, note that the scavenging activities of the polymer matrix containing tertiary amines (dimethylamino-G-gel) were not negligible. In addition to polyphenols, tertiary amines can participate to a certain extent in the peroxyl radical scavenging process of the CAT and GAL polymers. Further, the scavenging activities of all chelator-containing polymers decreased with time, probably as a result of the scavenging site saturation.

3.3.3. In Vitro Cytotoxicity

To confirm the safety of the prepared polymers for the in vivo experiments, their cytotoxicity was tested. The polymer beads are insoluble in an aqueous environment and nonabsorbable in the GIT. However, they can potentially contain trace amounts of water-soluble residues, which can cause a cytotoxic effect. Therefore, we designed a study inspired by the methods described in ISO 10993-5:1992.[47] In this study, polymer aqueous extracts of high concentrations were tested for cytotoxicity using the MTT assay. Here, a decrease of cell viability by more than 30% was considered a cytotoxicity sign. The results indicate that all prepared polymers show a negligible to nonexistent cytotoxic effect on the cells (Figure S5, Supporting Information). Furthermore, the cells in the GIT are protected by a luminal layer of mucins, which naturally increase the safe exposure limit of xenobiotics for the GIT cells.[48,49] Moreover, the effect of the prepared materials on the surrounding tissues was further confirmed by a robust in vivo histological examination (see Section 3.4).

3.4. In Vivo Experiments

3.4.1. Biodistribution of the Polymer per os

The polymer biodistribution was tested to confirm the nonabsorbability of the polymer from the GIT, and to determine the polymer retention capability in GIT, which is an important factor for the intended application. The synthesized ^{125}I-labeled CAT polymer was used for the study of in vivo biodistribution. The biodistribution of the CAT, GAL, and FEN polymers is expected to negligibly differ as their biodistribution is mostly size-dependent, and the particle size distribution is the same for all polymers, which is provided by the same starting material G-gel (see Section 3.1).

A suspension of the ^{125}I-labeled CAT polymer was directly administered to the mice stomach ($n = 4$), and the SPECT and CT images were performed at various time intervals, to 56 h after administration (**Figure 4**A). The data suggested that the polymer forms a depot in the stomach, and is then slowly released in the small intestine. This is may be caused by the cationic nature of the particles and the anionic nature of the mucin on the gastric and duodenal mucosa. The biological polymer half-life (assuming that it follows pseudo-first order kinetics) was estimated to be 5.5 ± 1.8 h in the stomach and 6.5 ± 2.0 h in the entire GIT (see Sections S5 and S6 and Figures S18–S22 in the Supporting Information). This prolonged retention is advantageous for the intended application since the prolonged polymer retention in the stomach and GIT increases the time of availability for the metal complexation after a single per os administration. The polymer retention, however, increases the necessity of low toxicity and low pro-oxidant properties of the polymer to prevent any damage to GIT over a long-term treatment. The plot of the total (whole body) detected activity as a function of time can be seen in Figure S23 in the Supporting Information.

Here, the SPECT images served as an illustrative spatial visualization of the polymer biodistribution. Theoretically, the polymer amount present in the organs can be quantified

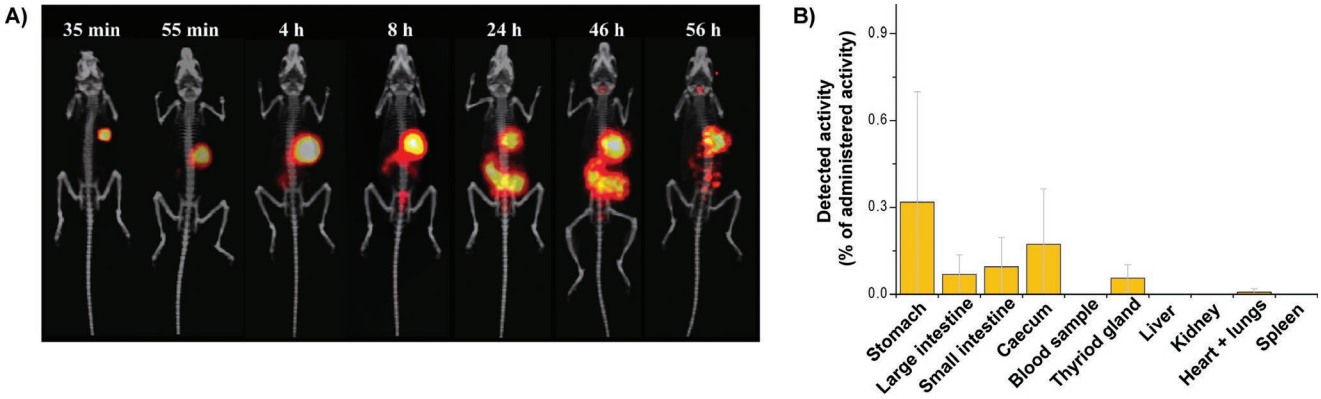

Figure 4. A) Merged images from the SPECT camera and CT in various time intervals after the radioactive polymer administration. Note that the activity is shown as a relative hotspot distribution in each frame to show the relative organ distribution (see Sections S5 and S6 in the Supporting Information). The plot of the total detected activity as a function of time can be seen in Figure S23 in the Supporting Information. B) Total relative ex vivo activity (decay-corrected) in mice 58 h after the administration. The quantification limit was 370 Bq (less than 0.001% of the administered activity).

according to the detected activity (Figure S23, Supporting Information). ^{125}I emits mostly 27 and 35 keV X-rays [50] which have relatively low energies, and thus, they are absorbed to a high extent by the surrounding tissue. Total detected activity is dependent on the source geometry (organ shape).

Therefore, ex vivo biodistribution was determined to refine the obtained SPECT results (Figure 4B). A negligible activity was detected in the thyroid gland, which probably caused by the minor polymer microbial deiodination in gastrointestinal tract[51] with following free iodide uptake rather than a spontaneous hydrolysis of the polymer. This reaction is catalyzed by iodotyrosine deiodinase enzyme from bacteria that is present in mice intestine.[52,53] A minor activity was also monitored in the lungs of one mouse, which was probably caused by the polymer aspiration during the administration. Apart from these, no activity occurred outside the gastrointestinal tract (and all can be explained) which indicates a nonabsorbability of the polymer from the GIT. Furthermore, the data suggests that the polymer remains in the GIT for a long time (Figures S18–S23, Supporting Information).

3.4.2. Iron Uptake Suppression by the Prepared Polymers

The CAT and FEN polymer chelators were selected for the in vivo experiments due to their excellent in vitro results.

First, the mice feed, which contained 35.00 ± 3.85 mg iron per kilogram of feed, was prepared. This value is consistent with the recommended iron concentration in the mice feed,[54] and are also relevant to the concentrations of iron in a common human diet.[27,55] The final mixture also contained the recommended amounts of other metals for mice feed.[54] Thereafter, the prepared FEN (15.63 g kg^{-1} feed) and CAT (5.85 g kg^{-1} feed) polymers were added to this prepared mice feed. The amount of added CAT polymer was designed to chelate all iron ions in the feed (25-fold molar excess of chelating groups compared with iron ions, based on data in Figure 2 and with regard to Table 2). The addition of FEN polymer was targeted to have the same molar amount of chelating groups in the feed in both groups. However, FEN polymer contains almost sevenfold fewer chelating groups compared to CAT, thus, the theoretical amount of added FEN (40.6 g kg^{-1} feed) would be too high for real application, and therefore a smaller amount of FEN was used. Nevertheless, FEN chelating moieties were still in a significant excess over iron ions (tenfold molar excess).

The mice were randomly divided into 3 groups and were fed with the prepared diets with the CAT (chelator of mainly Fe^{3+}), FEN (chelator of both Fe^{2+} and Fe^{3+}), or no polymer addition (control group). The mouse weight, hematocrit, and hemoglobin levels were monitored (**Figure 5**). Most iron from diet is not absorbed from GIT and remains in feces; our polymers limit the fraction of uptaken iron (which is, however, a minor part of iron in diet). Therefore, the overall content of iron in feces rises only negligibly, and so the content of iron in the feces is not a reliable indicator of the efficacy of the therapy. The iron content in urine (unless small-molecule chelators or "nanochelators"[57] are administered or blood in urine is present) is negligible.[2,7,8] For this reason, both the hemoglobin level and the hematocrit levels are the indicators of the iron supply in the body; the weight is an indicator of the mice fitness (major pathologies could decrease the mouse weights). In previous studies with female BALB/c mice, hemoglobin levels above 139 g L^{-1} were considered normal, 128–138 g L^{-1} were considered very mildly anemic, 110–127 g L^{-1} mildly anemic, 93–109 g L^{-1} moderately anemic, and 75–92 g L^{-1} were considered severely anemic in female C57BL/6 mice.[56] This experiment was designed to reveal both the efficacy of the polymer-based treatment and the possible subchronic toxicity.

The blood samplings were intentionally higher for the first 20 days to deplete the natural iron supply. Thus, both the hemoglobin level and the hematocrit level decreased significantly during the first 20 days in each groups. Within the next 10 days, the hemoglobin levels increased in the control group to a physiological level and remained at this level until the end of the experiment. In the FEN- and CAT- treated groups, the recovery of the hemoglobin and hematocrit levels was significantly slower than in the control group. Moreover, the hemoglobin and hematocrit levels remained significantly decreased in the FEN-treated group until the end of the experiment (could be classified as a mild anemia). Due to the induced anemia

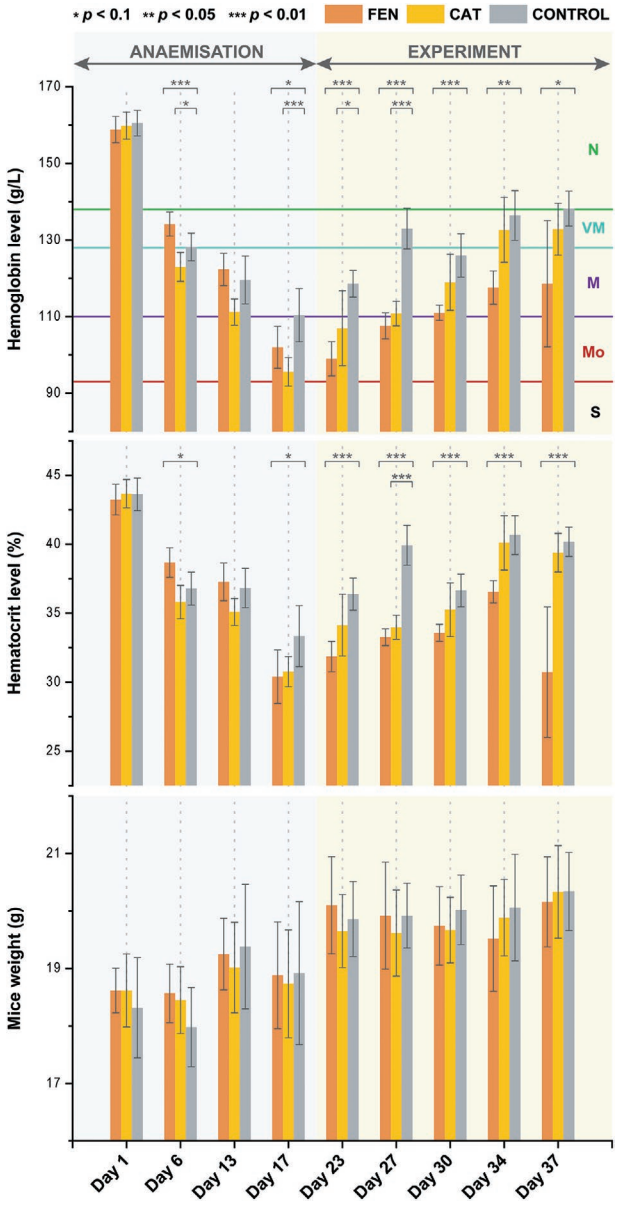

Figure 5. Hemoglobin levels, hematocrit levels, and mice weight of all groups as a function of time. All values presented as average ± SD; outlier values were excluded. Normal hemoglobin (N, ≥139 g L^{-1}), very mildly anemic (VM, 128–138 g L^{-1}), mildly anemic (M, 110–127 g L^{-1}), moderately anemic (Mo, 93–109 g L^{-1}), and severely anemic (S, 75–92 g L^{-1}) levels were indicated by the horizontal lines.[56]

in mice, their erythrocytes were both smaller in diameter and decreased in number (microcytic anemia). Therefore, the hematocrit levels were burdened with a larger error, thus, the hemoglobin level is more reliable marker of iron levels.

The hemoglobin and hematocrit levels indicate that both the FEN and CAT polymers decreased the biological availability of iron from the feed. However, the exact quantification of this effect is impossible, as an unknown amount of iron was stored mainly inside the mouse liver and spleen from the beginning of the experiment. These organ iron reservoirs served as one of the iron sources for hemoglobin synthesis even if no iron was absorbed from the feed. FEN polymer exhibited a significantly greater efficacy despite its lower content in chelating groups. This result may be attributed to the higher affinity of 1,10-phenanthroline moiety toward Fe^{2+} ions, which have a higher biological availability then Fe^{3+}. The chelation of Fe^{3+} ions with CAT polymer caused a statistically significant decrease of iron absorption; however, the effect was weaker than that of the FEN-treated group. This result indicates the necessity of the Fe^{2+} chelation to attain a better therapeutic effect.

Moreover, the mice weights in all groups slowly and steadily increased, and no significant weight loss, weight gain nor any other significant behavior and feeding pattern difference between the groups of experimental animals was observed.

On day 41, the mice were sacrificed via diethyl ether anesthesia overdosing and the histological examination of kidneys, hearts, stomachs, small intestines, colons, and spleens showed no difference between the control and the polymer-treated groups (**Figure 6**). The only slight difference from others was for the FEN-treated group, however, this was only a sampling issue as neither specific pathological findings nor any distinctive changes in cytoarchitecture or tissue integrity were observed in all vital organs, which shows neither local toxicity of the polymers nor systemic toxicity of the polymers. The differences in organ samples' appearances were caused merely by the sampling (e.g., in colon and heart), the findings are physiological in all cases. Interestingly, the chyme in stomach and small intestine contains visible traces of the chelating polymer (red spheres).

4. Conclusions

We have synthesized iron-chelating polymers and demonstrated their therapeutic potential for the maintenance and/or preventive therapy of hereditary hemochromatosis and/or other diseases with similar pathology in a comprehensive set of experiments. After the initial reduction of excessive iron from the body by means of phlebotomy, these polymers give a great advantage over the currently used maintenance therapy.

These polymers were prepared in the form of small beads larger than 15 µm. This size was shown to be sufficient for preventing polymer absorption after per os administration from the GIT (confirmed by in vivo biodistribution study), while still sufficiently small to provide a reasonably fast iron chelation. All polymers (CAT, FEN, and GAL) exhibited a remarkably fast chelation of Fe^{3+} ions; one polymer was shown to chelate the Fe^{2+} as well as Fe^{2+} ions. The polymers were reasonably selective as shown by both in vitro experiments and in silico simulations. Moreover, the polymers were noncytotoxic, and all (except for GAL) exhibit antioxidant behavior. The polymer therapeutic efficacy was demonstrated in a subchronic toxicity study in mice. The hematocrit and hemoglobin levels in the polymer-treated mice groups were significantly lower than those in the control group, which indicates a decrease in the biological availability of iron in the treated groups. The FEN polymer with affinity toward both Fe^{2+} and Fe^{3+} exhibited greater efficacy than CAT polymer exhibiting affinity predominantly toward Fe^{3+} ions. The histological examination revealed no pathology in the gastrointestinal tract or any other vital organs.

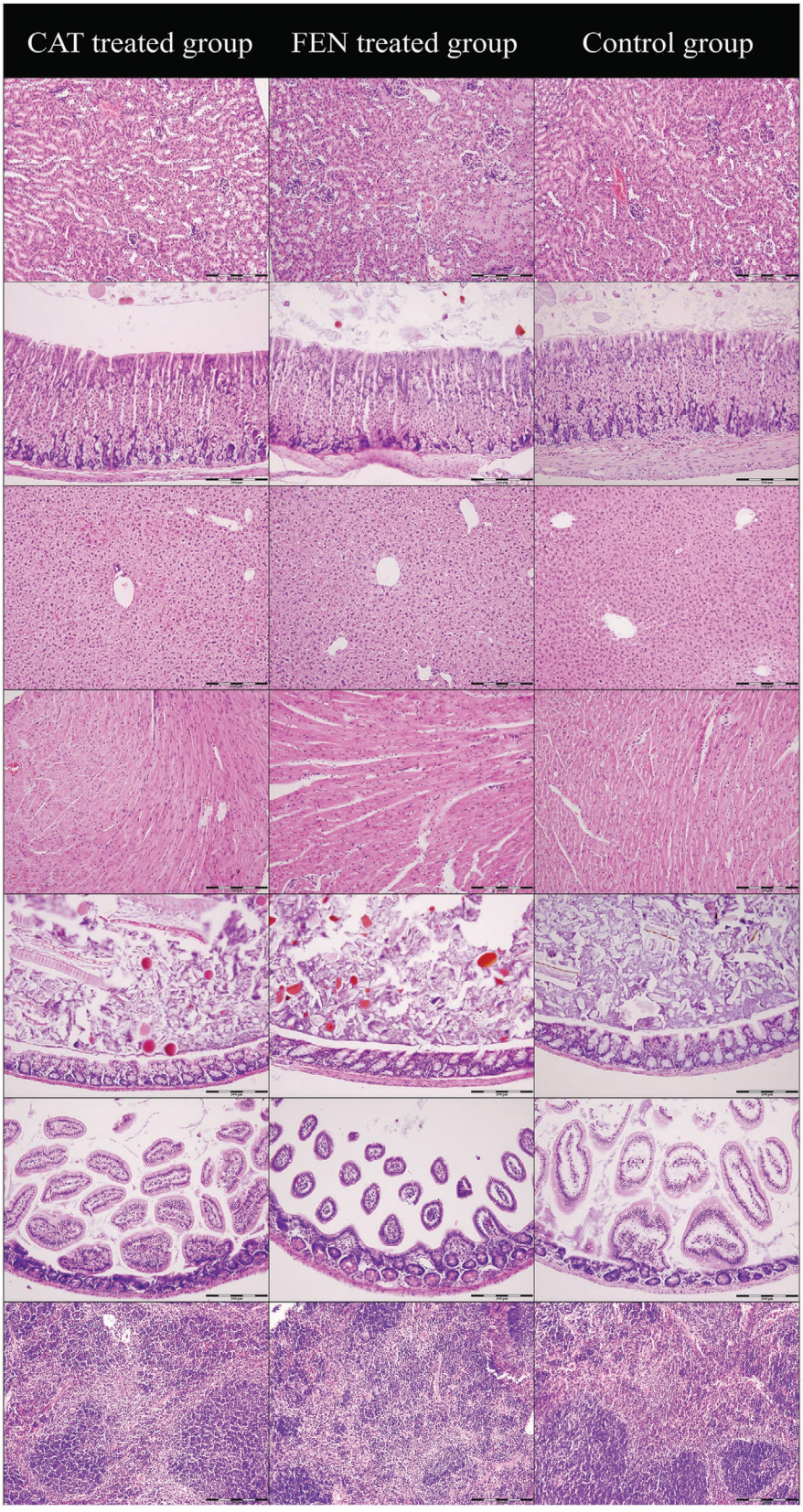

Figure 6. Histological evaluation of polymer-treated mice and control group (day 41). Samples were stained with hematoxylin and eosin; magnification: 200-fold. No pathology or difference between the testing groups was observed in any organ.

This study contains several key results, which could improve the polymer-based therapy and enable its use as the next-generation maintenance (or preventive) therapy for hereditary hemochromatosis and/or diseases with similar pathology. We provide a feasible guide (including in silico methods) for rational-design development of new chelating polymers with superior biodistribution, chelation capacity and selectivity, and no local or systemic toxicity.

Supporting Information

Supporting Information is available from the Wiley Online Library or from the author.

Acknowledgements

The authors acknowledge the assistance of Jana Šrotýřová in the performance of in vitro experiments to determine the polymer antioxidant properties. The authors acknowledge the financial support from the Czech Science Foundation (Grant Nos. 19-01438S (P.Št, M.H., and O.G.) and 19-27454V (V.M.M. and P.H.)), from the Ministry of Education, Youth and Sports of the Czech Republic (National Sustainability Program NPU I, project POLYMAT # LO1507). The authors acknowledge the financial support from the Grant Agency of Charles University (Project Nos. 602119 and 766119; K.K., P.Šv, and O.G.). The in vivo experiments in CAPI were supported by the Ministry of Education, Youth and Sports of the Czech Republic (Large RI Project LM2018129 Czech-BioImaging), by Charles University (SVV 260519/2020), and by the European Regional Development Fund (Project No. CZ.02.1.01/0.0/0.0/16_013/0001775). Access to computing and storage facilities provided under the programs "Projects of Large Research, Development, and Innovations Infrastructures" CESNET LM2015042 and CERIT Scientific Cloud LM2015085 is greatly appreciated.

Conflict of Interest

The authors declare no conflict of interest.

Author Contributions

O.G., L.P., P.H., and M.H. conceptualized the project. Investigation was carried out by O.G., L.P., K.K., P.Šv., V.M.M., J.Ku., P.P., M.B., T.H., R.P., and J.C. O.G., L.P., K.K., P.Šv., L.L., V.M.M., J.Ku., J.Kr and J.C. were involved in the data curation. Formal analysis was carried out by O.G., L.P., and L.L. O.G., L.P., K.K., P.Šv., L.L., P.F., J.K., J.K., P.P., M.B., T.H., R.P., J.C., and P.Št. were involved in the methodology. O.G., P.F., and J.Ku. were involved in project administration. Validation was carried out by O.G., L.P., P.Š., L.L., and M.H., and O.G. and L.L. helped with visualization. O.G., L.P., K.K., P.Šv., and M.H. wrote and prepared the original draft. O.G., L.P., L.L., and M.H. were involved in writing, review, and editing of the paper. L.P., R.P., L.Š., J.B., P.Št., P.H., and M.H. helped with the resources. K.K., P.Šv., L.Š., J.B., P.Št., and M.H. were involved in funding acquisition. D.D. and P.H. helped with the software. P.Šv. and M.H. did the supervision.

Keywords

antioxidant, experimental therapy, hemochromatosis, iron metabolism, iron overload, maintenance therapy, polymeric chelator, preventive therapy, siderophore, SPECT, uptake inhibitor

Received: July 22, 2020
Revised: August 27, 2020
Published online:

[1] W. J. H. Griffiths, *Medicine* **2011**, *39*, 597.
[2] A. Pietrangelo, *Gastroenterology* **2010**, *139*, 393.
[3] P. C. Adams, J. C. Barton, *Lancet* **2007**, *370*, 1855.
[4] M. Betts, P. A. Flight, L. C. Paramore, L. Tian, D. Milenković, S. Sheth, *Clin. Ther.* **2020**, *42*, 322.
[5] F. M. O'Reilly, C. Darby, J. Fogarty, W. Tormey, E. W. Kay, M. Leader, G. M. Murphy, *Arch. Dermatol.* **1997**, *133*, 1098.
[6] C. Q. Edwards, J. P. Kushner, *N. Engl. J. Med.* **1993**, *328*, 1616.
[7] R. J. Simpson, A. T. McKie, *Cell Metab.* **2009**, *10*, 84.
[8] P. Brissot, M.-B. Troadec, E. Bardou-Jacquet, C. Le Lan, A.-M. Jouanolle, Y. Deugnier, O. Loreal, *Blood Rev.* **2008**, *22*, 195.
[9] R. E. Fleming, P. Ponka, *N. Engl. J. Med.* **2012**, *366*, 348.
[10] H. Kondo, K. Saito, J. P. Grasso, P. Aisen, *Hepatology* **1988**, *8*, 32.
[11] E. Beutler, *Blood* **2003**, *101*, 3347.
[12] P. Adams, A. Altes, P. Brissot, B. Butzeck, I. Cabantchik, R. Cançado, S. Distante, P. Evans, R. Evans, T. Ganz, *Hepatol. Int.* **2018**, *12*, 83.
[13] C. J. Gallego, A. Burt, A. S. Sundaresan, Z. Ye, C. Shaw, D. R. Crosslin, P. K. Crane, S. M. Fullerton, K. Hansen, D. Carrell, *Am. J. Hum. Genet.* **2015**, *97*, 512.
[14] J. Alexander, K. V. Kowdley, *Genet. Med.* **2009**, *11*, 307.
[15] A. Åsberg, K. Hveem, K. Thorstensen, E. Ellekjaer, K. Kannelønning, U. Fjøsne, T. B. Halvorsen, H.-B. Smethurst, E. Sagen, K. S. Bjerve, *Scand. J. Gastroenterol.* **2001**, *36*, 1108.
[16] S. Distante, J. P. Berg, K. Lande, E. Haug, H. Bell, *Scand. J. Gastroenterol.* **1999**, *34*, 529.
[17] H. A. Jackson, K. Carter, C. Darke, M. G. Guttridge, D. Ravine, R. D. Hutton, J. A. Napier, M. Worwood, *Br. J. Haematol.* **2001**, *114*, 474.
[18] R. Sood, R. Bakashi, V. S. Hegade, S. M. Kelly, *Br. J. Gen. Pract.* **2013**, *63*, 331.
[19] T. P. Flaten, J. Aaseth, O. Andersen, G. J. Kontoghiorghes, *J. Trace Elem. Med. Biol.* **2012**, *26*, 127.
[20] J. C. Barton, *Lancet Haematol.* **2017**, *4*, e569.
[21] P. Brissot, S. Ball, D. Rofail, H. Cannon, V. W. Jin, *Transfusion* **2011**, *51*, 1331.
[22] B. Galy, D. Ferring-Appel, S. Kaden, H.-J. Gröne, M. W. Hentze, *Cell Metab.* **2008**, *7*, 79.
[23] D. Roberts, S. Brunskill, C. Doree, S. Williams, J. Howard, C. Hyde, *Cochrane Database Syst. Rev.* **2007**, *3*, CD004839.
[24] J.-I. Henter, J. Karlén, *Blood* **2007**, *109*, 5157.
[25] M. D. Cappellini, A. Cohen, A. Piga, M. Bejaoui, S. Perrotta, L. Agaoglu, Y. Aydinok, A. Kattamis, Y. Kilinc, J. Porter, *Blood* **2006**, *107*, 3455.
[26] European Association for the Study of the Liver, *J. Hepatol.* **2010**, *53*, 3.
[27] Z. K. Roughead, J. R. Hunt, *Am. J. Clin. Nutr.* **2000**, *72*, 982.
[28] T. J. Peters, K. B. Raja, R. J. Simpson, *Food Chem.* **1992**, *43*, 315.
[29] J. D. Cook, E. R. Monsen, *Am. J. Clin. Nutr.* **1977**, *30*, 235.
[30] M. A. Bryszewska, *Nutrients* **2019**, *11*, 273.
[31] J. Qian, B. P. Sullivan, S. J. Peterson, C. Berkland, *ACS Macro Lett.* **2017**, *6*, 350.
[32] T. Zhou, H. Neubert, D. Y. Liu, Z. D. Liu, Y. M. Ma, X. L. Kong, W. Luo, S. Mark, R. C. Hider, *J. Med. Chem.* **2006**, *49*, 4171.
[33] S. C. Polomoscanik, C. P. Cannon, T. X. Neenan, S. R. Holmes-Farley, W. H. Mandeville, P. K. Dhal, *Biomacromolecules* **2005**, *6*, 2946.
[34] S. Grimme, S. Ehrlich, L. Goerigk, *J. Comput. Chem.* **2011**, *32*, 1456.
[35] A. S. Lileev, V. L. Dar'ya, A. K. Lyashchenko, *Mendeleev Commun.* **2007**, *17*, 364.

[36] Turbomole, A Development of University of Karlsruhe and Forschungszentrum Karlsruhe GmbH, 1989–2007, Turbomole GmbH **2007**, http://www.turbomole.com
[37] J. Řezáč, *J. Comput. Chem.* **2016**, *37*, 1230.
[38] ISO/IEC 17025:2005, International Organization for Standardization **2005**.
[39] F. Švec, J. Hradil, J. Čoupek, J. Kálal, *Angew. Makromol. Chem.* **1975**, *48*, 135.
[40] J. S. Thompson, J. C. Calabrese, *J. Am. Chem. Soc.* **1986**, *108*, 1903.
[41] K. Tomita, Y. Takashi, Y. Ouchi, Y. Kuwahara, K. Igarashi, T. Nagasawa, H. Nabika, A. Kurimasa, M. Fukumoto, Y. Nishitani, *Cancer Sci.* **2019**, *110*, 2856.
[42] S. B. Nimse, D. Pal, *RSC Adv.* **2015**, *5*, 27986.
[43] J. Lü, P. H. Lin, Q. Yao, C. Chen, *J. Cell. Mol. Med.* **2010**, *14*, 840.
[44] G. P. Bienert, J. K. Schjoerring, T. P. Jahn, *Biochim. Biophys. Acta, Biomembr.* **2006**, *1758*, 994.
[45] G. Spiteller, *Free Radical Biol. Med.* **2006**, *41*, 362.
[46] D. Huang, B. Ou, M. Hampsch-Woodill, J. A. Flanagan, R. L. Prior, *J. Agric. Food Chem.* **2002**, *50*, 4437.
[47] ISO 10993-5:1992, International Organization for Standardization **1992**.
[48] M. E. V. Johansson, H. Sjövall, G. C. Hansson, *Nat. Rev. Gastroenterol. Hepatol.* **2013**, *10*, 352.
[49] G. C. Hansson, *Curr. Opin. Microbiol.* **2012**, *15*, 57.
[50] J. Katakura, M. Oshima, K. Kitao, H. Iimura, *Nucl. Data Sheets* **1993**, *70*, 217.
[51] E. Fröhlich, R. Wahl, *Trends Endocrinol. Metab.* **2019**, *30*, 479.
[52] A. Querido, J. B. Stanbury, A. A. H. Kassenaar, J. W. A. Meijer, *J. Clin. Endocrinol. Metab.* **1956**, *16*, 1096.
[53] M. M. Häggblom, I. D. Bossert, *Microbial Processes and Environmental Applications*, Springer, New York **2003**.
[54] National Research Council, *Nutrient Requirements of Laboratory Animals*, National Academies Press, Washington, DC **1995**.
[55] T. H. Bothwell, R. D. Baynes, B. J. MacFarlane, A. P. MacPhail, *J. Intern. Med.* **1989**, *226*, 357.
[56] B. M. Raabe, J. E. Artwohl, J. E. Purcell, J. Lovaglio, J. D. Fortman, *J. Am. Assoc. Lab. Anim. Sci.* **2011**, *50*, 680.
[57] H. Kang, M. Han, J. Xue, Y. Baek, J. Chang, S. Hu, H. Nam, M. J. Jo, G. E. Fakhri, M. P. Hutchens, H. S. Choi, J. Kim, *Nat. Commun.* **2019**, *10*, 5134.
[58] O. Groborz, *BSc Thesis*, Charles University **2019**.